AIAA JOURNAL
Vol. 57, No. 3, March 2019

Do Epistemic Uncertainties Allow for Replacing Microstructural Experiments with Reconstruction Algorithms?

Pınar Acar*
Virginia Polytechnic Institute and State University, Blacksburg, Virginia 24061
and
Veera Sundararaghavan†
University of Michigan, Ann Arbor, Michigan 48109

DOI: 10.2514/1.J057488

A novel problem in computational materials modeling is addressed: "Are the computational microstructure reconstruction techniques reliable enough to replace experiments?" Here, "reliable" computations are associated with producing "expected" reconstructions that are adequately close to the experimental data. The output of computational techniques can deviate from the experimental measurements because of the epistemic uncertainties in the algorithms. In this work, an analytical formulation for quantification of epistemic uncertainties in a microstructure reconstruction algorithm based on Markov random field is presented. The method is used to predict the large-scale spatial distribution of a microstructure given an experimental input measured over a small spatial domain. However, small variations are observed on the microstructural features of the synthesized samples due to the Markov random field algorithm. The proposed analytical technique aims to quantify these uncertainties and estimate their propagation to the macroscale material properties to provide a significant understanding on how reliable it is to replace the experiments with the Markov random field model to predict microstructural maps over large spatial domains.

Nomenclature

A	=	orientation distribution function
C	=	stiffness matrix, GPa
E	=	experimental microstructure
G	=	coloring level
L	=	lattice
N_{nodes}	=	number of independent nodes
N	=	number of samples
N_{elem}	=	number of finite elements
N_f	=	number of failed samples
N_{int}	=	number of integration points
P_f	=	probability of failure
p	=	property matrix
q	=	volume normalization vector
r	=	Rodrigues vector
S	=	synthesized microstructure
S_ν	=	colors of pixels in synthesized image
X	=	color variable
β	=	reliability index
μ_A	=	mean values of orientation distribution function
ν	=	pixel
ω	=	Gaussian weight function
Σ_A	=	covariance matrix for orientation distribution function
σ_y	=	yield stress, MPa

I. Introduction

COMPUTATIONAL models using deterministic parameters have been traditionally in use to study microstructural features and link these features to macroscale material properties. However, none of the computational models can produce an output that provides a 100% match with the test data. This is because of the uncertainties that are arising from "lack of knowledge" such as inaccuracies, errors, or assumptions in computations. Such uncertainties are categorized as "epistemic uncertainties" and they are independent from the variations that are seen due to the stochastic nature of microstructures. The stochastic behavior is associated with the aleatoric uncertainty, which is an irreducible variation that is naturally present in the system. The aleatoric uncertainties can be quantified by analyzing the experimental data, and they can propagate to the larger scales randomly. However, the epistemic uncertainty is an aspect of the computational model in use, and it is usually very hard to distinguish it from the aleatoric uncertainty. The uncertainties in physical systems can alter the expected performance of the material systems. This is especially very important for aerial vehicles that are highly sensitive to the material features. The variations in the material properties caused by the small-scale (microscopic level) uncertainties can lead to severe problems, including failure of the vehicle. To achieve reliable designs for aerial vehicles, the stochasticity introduced in the computational models should be modeled (Fig. 1). The reliability of the designs can then be defined using the probability distributions of the output parameters. Because of its critical role in modeling and design, the uncertainty quantification (UQ) has been a growing field in aerospace engineering.

The present study addresses a UQ methodology to study the effect of epistemic uncertainties for metallic materials that are used in aerospace vehicles. First, the verification of the UQ approach will be performed for copper. Next, the UQ technique will be studied comprehensively for a titanium–aluminum alloy (Ti-7Al), which is a widely preferred alloy in aerospace engineering owing to its high strength, excellent corrosion resistance, and high temperature stability [1]. In this work, the uncertainties in the material system are introduced by a microstructure reconstruction algorithm, which generates larger-scale microstructural data by using the available small-scale data. The reconstruction problem helps the engineers avoid the expensive large-scale measurements. With the integration of a reconstruction strategy, larger-scale data become available by using the test data measured at a smaller-scale domain. One of the goals in this work is to implement a Markov random field (MRF)–based reconstruction study to achieve the large-scale data of microstructures. Here, the readers are referred to Ref. [2] for the fundamental aspects of the MRFs. The MRF technique introduces epistemic uncertainties to the system because of the algorithmic

Received 9 May 2018; accepted for publication 3 October 2018; published online 8 January 2019.

*Assistant Professor, Department of Mechanical Engineering. Member AIAA.
†Associate Professor, Department of Aerospace Engineering. Member AIAA.

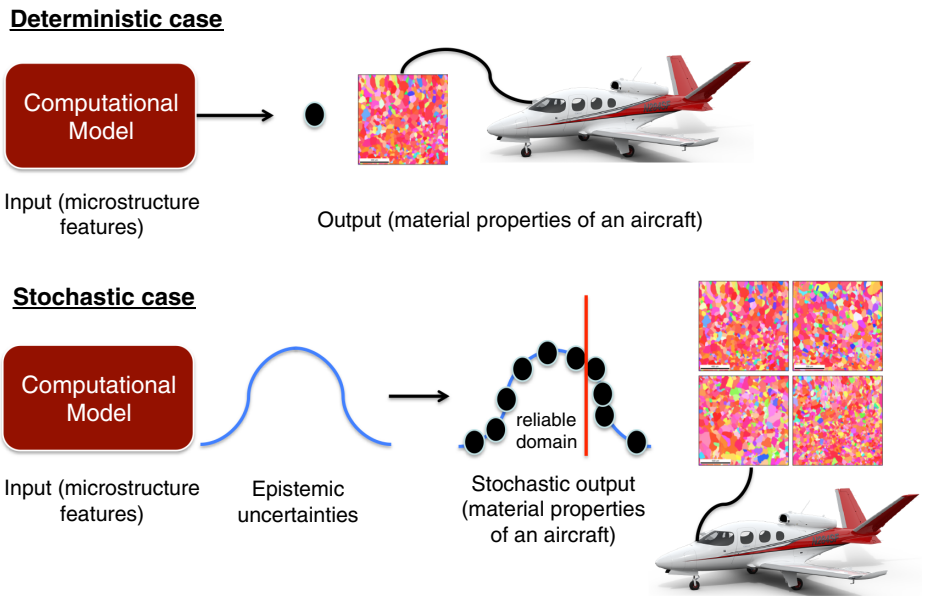

Fig. 1 Comparison of deterministic and stochastic analyses for aerospace materials. The deterministic designs are not able to examine the model uncertainties. However, these epistemic uncertainties can be modeled with a stochastic computational approach. In stochastic modeling, the output parameters, such as the material properties of an aircraft (e.g., yield strength, stiffness), are stochastic as well.

randomness. These uncertainties can affect the overall accuracy of the algorithm and thus the desired material properties and structural performance. Therefore, we check the accuracy of the MRF-based reconstruction strategy by comparing the results to the available experimental measurements. However, another aspect appears here: the experiments are performed on the different parts of the same material and they predict a range for material properties rather than a deterministic property value. This experimental variability is known as aleatoric uncertainty and it is conceptually different from the epistemic uncertainty. Here, to distinguish the epistemic uncertainties (model uncertainty) from the aleatoric uncertainties (experimental uncertainty), the experimental prediction regions are assumed to be 100% reliable. Thus, the MRF-based computational algorithm is assumed to be reliable if it estimates a material property value within the experimental ranges. Any computational result that is not a subspace of the experimental prediction domain is assumed to occur because of the epistemic uncertainties in the algorithm. This is a novel problem in computational materials modeling because the epistemic uncertainties have not been independently studied in the community yet to the best of authors' knowledge. Instead, the UQ problem has only been solved for aleatoric uncertainties in the literature. The aleatoric uncertainties have been mostly modeled by using computational UQ techniques such as Monte Carlo simulation (MCS), polynomial chaos expansion (PCE), and stochastic collocation (SC). For example, Creuziger et. al. [3] used MCS to examine the uncertainties in the microstructures that are introduced by the variations in the pole figure data. Kouchmeshky and Zabaras [4] presented the propagation of initial texture and deformation process uncertainties on the final product properties. They used a data-driven approach to identify the joint probability distributions of random variables with maximum entropy method, and modeled the stochastic problem using the SC approach. These computational methods presented in literature employ a numerical algorithm for quantification and propagation of aleatoric uncertainties. They represent the joint probability distributions of uncertain variables either using interpolation functions or sampling for random points. These techniques are not very computationally efficient because, as the problem complexity or the number of variables increases, the number of interpolation terms or sampling points should also increase. Another drawback is the difficulty of satisfying strict design constraints (such as unit volume fraction) using the joint probability distributions of the numerical approaches. Because of all these disadvantages arising from the use of computational UQ techniques, an analytical UQ formulation has been previously presented by the authors to model the aleatoric uncertainties in microstructures [5–7].

In the present work, the analytical UQ formulation is extended to study the effect of epistemic uncertainties in the MRF-based microstructure reconstruction algorithm. The MRF model predicts the evolution of synthetic microstructures over large spatial domains given an experimental input. In this computational model, the "texture synthesis" is performed as the first step. Different windows taken from a polycrystalline microstructure generally "look alike." In mathematical terms, this amounts to the presence of a stationary probability distribution from which various microstructural snapshots are sampled. There are various ways of modeling this probability distribution indirectly. Feature-based algorithms have long been used that categorize various microstructural snapshots based on a common set of underlying features, and generate new synthetic images with similar features [8–10]. These features could include marginal histograms [8], multiresolution filter outputs (Gaussian [9] and wavelet [10] filters), and point probability functions (e.g., autocorrelation function) [11]. These methods are good at capturing the global features of the image; however, local information in the form of per-pixel data is lost. Thus, features such as grain boundaries are smeared out when reconstructing polycrystalline structures [10]. Alternatively, one could start with sampling the conditional probability density for the state of a pixel given the known states of its neighboring pixels using reference 2D or 3D experimental images. If only the nearest neighbors are chosen, this amounts to sampling from an Ising-type model [12]. For general microstructures, the correlation lengths can span several pixels [11] and a larger neighbor window may be needed. In this study, the generalized Ising models, called MRFs, are employed to model the spatial probability distribution. In Ising models, a lattice is constructed with pixels (with binary states) interacting with its nearest neighbors, whereas in MRFs, pixels take up integer or vector states and interact with multiple neighbors over a window. The sampling of conditional probability of a pixel given the states of its known neighbors is based on Claude Shannon's generalized Markov chain [13]. In the one-dimensional problem, a set of consecutive pixels is used as a template to determine the probability density function (PDF) of the next pixel. The study by Efros and Leung [14] developed a nonparameteric sampling approach for extending the sampling technique to 2D microstructures. In this approach, microstructures are grown layer by layer from a small seed image (3×3 pixels) taken randomly from the experimental micrograph. Here, the algorithm first finds all windows in an

experimental micrograph that are similar to an unknown pixel's neighborhood window. One of these matching windows is chosen and its center pixel is taken to be the newly synthesized pixel. This technique is popular in the field of texture synthesis [14–17] and in geological material reconstruction literature, where such sampling methods are termed "multiple-point statistics" [18], and more recently, it has been applied for modeling polycrystalline microstructures [19,20]. An alternate methodology based on optimization has become popular in recent years. The nonparameteric sampling method of Efros and Leung [14] is posed in the form of an expectation-maximization algorithm [21–23]. The approach minimizes a neighborhood cost function that ensures that the local neighborhood of the Ising lattice taken along the x, y, or z directions through the 3D microstructure is similar to some neighborhood in the 2D lattice imaged along that plane. This reconstruction problem leads to anisotropic microstructures that have similar high-order statistics [23], which is in contrast to other such works in literature that use assumptions of microstructural isotropy [24] or methods that use lower order statistics such as two-point correlation functions to synthesize 3D microstructures [25,26]. The sampling approach and the optimization approach can also be applied in tandem for various applications involving MRFs. The MRF model presented in this work has been studied before for predicting the spatiotemporal evolution of microstructures that are having different grain structures in our previous paper [20].

The synthesized microstructures with the MRF approach are quantified using an orientation distribution function (ODF), which measures the volumes of different orientations in a microstructure. The ODF is assigned as a mathematical parameter representing the microstructural features, and the epistemic uncertainties arising from the computational models are captured by modeling the variations in the ODFs. The analytical UQ algorithm is based on a Gaussian distribution approach [5–7], and here it can be implemented to study the epistemic uncertainties because the variations in the ODF values are found to be consistent with the Gaussian distribution. The analytical solution is also used to model the propagation of these uncertainties to the macroscale material properties such as stiffness and yield stress. The experimental electron backscatter diffraction (EBSD) samples of a titanium–aluminum alloy are used to predict the spatial evolution of the polycrystalline microstructure using the MRF model. Hundreds of synthesized images are generated to create sufficient statistics to analyze the uncertainties. The probability distributions of the material properties are then computed using the discrete MRF samples and analytical UQ algorithm. The analytical UQ algorithm is found to provide a very good estimate to the variations in the MRF samples. The material properties are also computed using the experimental EBSD samples. The material property values that are computed from the EBSD data have small variations due to the aleatoric uncertainties. These aleatoric uncertainties are eliminated from the epistemic uncertainties by defining the limits of the material properties that are predicted from the experimental data as reliable regions. Therefore any computational output that is not a subspace of the reliable region is assumed to occur because of the epistemic uncertainties. A mathematical reliability index approach is presented to define the similarity between the probability distribution of the analytical UQ method, and discrete experimental and MRF samples. The reliability analysis shows that the analytical model can accurately capture the variations arising from the epistemic uncertainties, and the epistemic uncertainties have a very little impact on the overall accuracy of the algorithm even though the algorithm predicts the spatial evolution in a larger domain. The high confidence levels show that the MRF algorithm should be a very strong candidate to replace the costly experimental data that are obtained with the measurements at large domains. The reliability analysis is also performed to model the effect of epistemic uncertainties when different window size parameters are used in the MRF model.

The findings of this study will make significant contributions to the computational materials modeling studies in the following aspects. First, it is shown that a computationally efficient analytical UQ model can be used to study not only the aleatoric uncertainties but also the epistemic uncertainties in microstructure modeling. This is the first time that an epistemic UQ problem has been addressed in the field to the best of authors' knowledge, and this problem has been handled by using a cost-effective analytical methodology. Therefore it has the potential to open up a new way in the community for studying the effect of epistemic uncertainties in common computational models/techniques that are used in microscale modeling and design. Second, the present work shows that to what extent the computational models can be reliably used to replace experimental data. This is studied by performing a mathematical reliability analysis that can define the similarity between continuous and discrete probability distributions and it concludes with an important suggestion on replacing costly experiments (or a portion of experiments) that are performed over larger spatial domains with computational reconstruction algorithms. The organization of the paper is as follows. The mathematical modeling aspects of the MRF approach and analytical UQ algorithm are discussed in Sec. II. An example is also studied in Sec. II to model the epistemic uncertainties when the input data are a cellular automata simulation output. In Sec. III, the epistemic uncertainties arising from the MRF approach when reconstructing synthesized samples from an experimental input are studied. A reliability index approach is also introduced to analyze the uncertainty results for different image and window sizes to provide a significant understanding on how much experimental data can reliably be captured by the MRF approach. The summary of the paper and suggestions for a potential future work are given in Sec. IV.

II. Mathematical Background

The mathematical modeling aspects of the MRF approach for generating synthesized microstructure samples and analytical UQ algorithm are discussed in this section. Section II.A briefly summarizes the fundamental features of the MRF approach as it was previously presented by the authors [20]. Section II.B gives brief information about the analytical UQ algorithm, which was employed to capture the aleatoric uncertainties in our previous works [5–7].

A. Mathematical Modeling of Microstructures as Markov Random Fields

Some of early attempts at microstructure modeling were based on Ising models [12]. In the Ising model, an $N \times N$ lattice (L) is constructed with values X_i assigned for each particle i on the lattice, $i \in [1, \ldots, N^2]$. In an Ising model, X_i is a binary variable equal to either $+1$ or -1 (e.g., magnetic moment [12]). In general, the values X_i may contain any one of G color levels in the range $\{0, 1, \ldots, G-1\}$ (following the integer range extension of the Ising model by Besag [27]). A *coloring* of L denoted by $\boldsymbol{X}$ maps each particle in the lattice L to a particular value in the set $\{0, 1, \ldots, G-1\}$. Ising models fall under the umbrella of *undirected graph models* in probability theory. To rewrite the Ising model as a graph, the neighbors to particles are assigned and the pairs of neighbors are linked using a bond as shown in Fig. 2a. The rule to assign neighbors is based on a *pairwise Markov property.* A particle j is said to be a neighbor of particle i only if the conditional probability of the value X_i, given all other particles [except (i, j), i.e., $p(X_i|X_1, X_2, \ldots, X_{i-1}, X_{i+1}, \ldots, X_{j-1}, X_{j+1}, \ldots, X_{N^2})$], depends on the value X_j.

Note that the above definition does not warrant the neighbor particles to be close in distance, although this is widely employed for physical reasons. For example, in the classical Ising model, each particle is bonded to the next nearest neighbor as shown in Fig. 2a. For modeling microstructures, a higher-order Ising model (Fig. 2b) can be used. The particles of the lattice correspond to pixels of the 2D microstructure image. The neighborhood of a pixel is modeled using a square window around that pixel and bonding the center pixel to every other pixel within the window. Using this graph structure, a *Markov random field* can be defined as the joint probability density $P(\boldsymbol{X})$ on the set of all possible colorings $\boldsymbol{X}$, subject to a *local Markov property.* The *local Markov property* states that the probability of value X_i, given its neighbors, is conditionally independent of the values at all other particles. In other words, $P(X_i|\text{all particles except } i) = p(X_i|\text{neighbors of particle } i)$. Next, a method based on Ref. [14] is

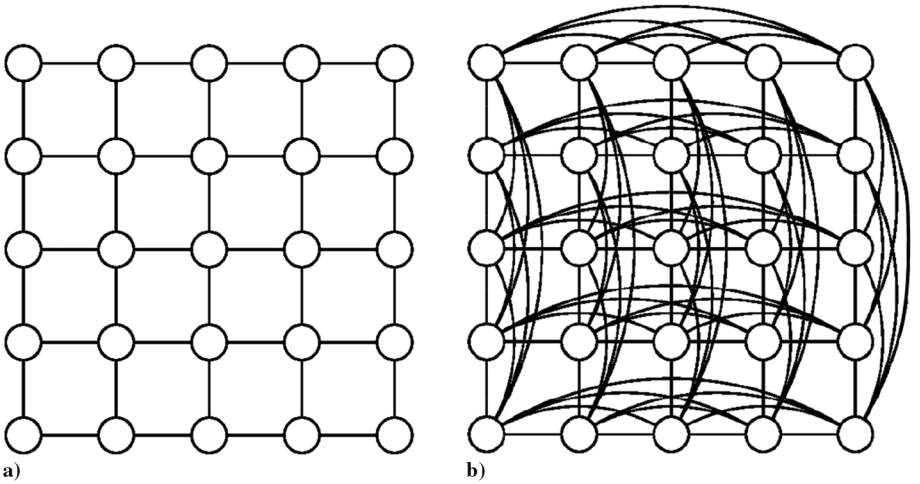

Fig. 2 MRF as an undirected graph model; circles are pixels in the image and bonds are used to connect neighbors: a) Ising model with nearest neighbor interactions. b) Microstructure modeled by including higher-order interactions in the Ising model.

described to sample from the conditional probability density $p(X_i|\text{neighbors of voxel } i)$.

In the following discussion, the color (X_i) of a pixel i is represented using G color levels in the range $\{0, 1, \ldots, G-1\}$ each of which maps to an RGB triplet. The number of color levels is chosen based on the microstructure to be reconstructed (e.g., for binary images $G = 2$). Let $\boldsymbol{E}$ and $\boldsymbol{S}$ denote the experimental and synthesized microstructure, respectively. Let v be a pixel in $\boldsymbol{S}$ whose color needs to inferred using the sampling procedure. Let $\boldsymbol{S}_v$ denote the colors in a neighborhood window around pixel v. Let $\boldsymbol{E}^w$ denote the colors of pixels in a window of the same size in the input 2D micrograph.

To find the coloring of pixel v, one needs to compute the conditional probability density $p(X_v|\boldsymbol{S}_v)$. Explicit construction of such a probability density is often computationally intractable. Instead, the most likely value of v is identified by first finding a window $\boldsymbol{E}_v$ in the input 2D micrograph that is most similar to $\boldsymbol{S}_v$ (see Fig. 3). This is done by solving the following problem (where $\boldsymbol{S}_{v,u}$ denotes the color of pixel u in $\boldsymbol{S}_v$ and $\boldsymbol{E}^w_u$ denotes the color of pixel u in $\boldsymbol{E}^w$):

$$\boldsymbol{E}_v = \arg\min_{\boldsymbol{E}^w} \sum_u \omega_{v,u}(\boldsymbol{S}_{v,u} - \boldsymbol{E}^w_u)^2 \tag{1}$$

where $D = \sum_u \omega_{v,u}(\boldsymbol{S}_{v,u} - \boldsymbol{E}^w_u)^2$ is a distance measure defined as the normalized sum of weighted squared differences of pixel colors. To preserve the short-range correlations of the microstructure as much as possible, the weight for nearby pixel is taken to be greater than pixels farther away (Gaussian weighting function ω is used). If the pixel u is located at position (x, y) (in lattice units) with respect to the center pixel v (located at $(0, 0)$), $\omega_{v,u}$ is given as:

$$\omega_{v,u} = \frac{\exp(-((x^2 + y^2)/2\sigma^2))}{\sum_i \sum_j \exp(-((i^2 + j^2)/2\sigma^2))} \tag{2}$$

Here, the summation in the denominator is taken over all the known pixels in $\boldsymbol{S}_v$. The weights $\omega_{v,u}$ for the unknown pixels in $\boldsymbol{S}_v$ are taken to be zero. This ensures that the distance measure is computed only using the known values and is normalized by the total number of known pixels. The standard deviation (σ) is taken to be $0.16w$. The problem in Eq. (1) is solved using an exhaustive search by comparing all the windows in the input 2D micrograph to the corresponding neighborhood of pixel v. In our approach, a measure of stochasticity is introduced by storing all matches with a distance measure that is within 1.3 times that of the best matching window [14]. The center pixel colors of all these matches give a histogram for the color of the unknown pixel (X_v), which is then sampled using a uniform random number.

The microstructure is grown layer by layer starting from a small seed image (3×3 pixels) taken randomly from the experimental micrograph (Fig. 3). In this way, for any pixel the values of only some of its neighborhood pixels will be known. The fundamental approximation in this numerical implementation is that the PDF of an unfilled pixel is assumed to be independent of the PDF of its unfilled neighbors. Each iteration in the algorithm involves coloring the unfilled pixels along the boundary of filled pixels in the synthesized

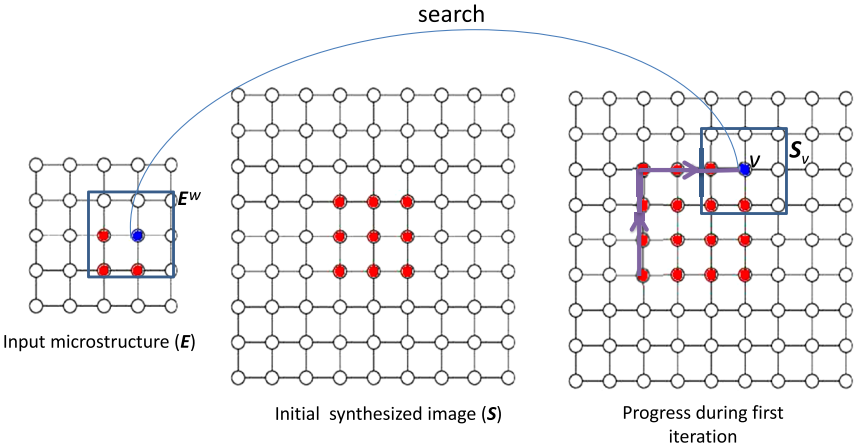

Fig. 3 The MRF approach [14,28]: The image is grown from a 3×3 seed image (center). As the algorithm progresses along the path shown (right), the unknown output pixel (shown in blue) is computed by searching for a pixel with a similar neighborhood in the input image (left).

image as shown in Fig. 3. An upper limit of 0.1 is enforced for the distance measure initially. If the matching window for a unfilled pixel has a larger distance measure, then the pixel is temporarily skipped while the other pixels on the boundary are filled. If none of the pixels on the boundary can be filled during an iteration, then the threshold is increased by 10% for the next iteration.

The window size is the only adjustable parameter for different microstructures. Window size plays an important role in the MRF model. At window sizes much smaller than the correlation lengths, false matches lead to high noise in the reconstructions. At very high window sizes, not enough matching windows can be identified. Hence, there is an ideal window size that needs to be found through numerical trial. More details about the effect of window size can be found in our previous work [20].

B. Analytical UQ Algorithm

The epistemic uncertainties arising from the reconstruction of the microstructural samples using the MRF approach are quantified using an analytical algorithm that was previously introduced in our earlier works [5–7]. The analytical UQ method is based on a Gaussian distribution approach. Given the input variations that can be represented with a Gaussian distribution, the propagation of the uncertainties is computed with the linear transformation feature of the Gaussian distribution for linear output parameters, and with transformation of variables rule for nonlinear output parameters. Similar to our previous works, the microstructure is quantified with the ODF. The ODF measures the volume fraction of different orientations in a microstructural space. The ODF values at each nodal point are discretized using a finite element approach in Rodrigues fundamental domain [29,30]. Discretizing the ODF in the Rodrigues space is advantageous because of the regularity of its geometry [29], which allows discretization of the space using finite elements. The ODF is discretized into N independent nodes with N_{elem} finite elements and N_{int} integration points per element. Using this parametrization, any polycrystal property can be expressed in a linear form [31] as in Eq. (3). A finite element integration scheme using Gauss quadrature allows matrix representation of Eq. (3).

$$\langle \chi \rangle = \int_R \chi(\boldsymbol{r}) \boldsymbol{A}(\boldsymbol{r})\, \mathrm{d}v = \sum_{n=1}^{N_{\text{elem}}} \sum_{m=1}^{N_{\text{int}}} \chi(r_m) A(r_m) w_m |J_n| \frac{1}{(1 + r_m \cdot r_m)^2} \tag{3}$$

where $A(r_m)$ is the value of the ODF at the mth integration point with global coordinate r_m of the nth element, $|J_n|$ is the Jacobian determinant of the nth element, w_m is the integration weight associated with the mth integration point, and $1/(1 + r_m \cdot r_m)^2$ represents the metric of Rodrigues parameterization. This can be shown to be equivalent to an equation linear in the ODF: $\langle \chi \rangle = \boldsymbol{p}^T \boldsymbol{A}$, where $\boldsymbol{A}$ is a column vector containing the ODF values at the k independent nodes of the ODF mesh [7]. In addition, the ODF is normalized to unity as $\boldsymbol{q}^T \boldsymbol{A} = 1$ where $\boldsymbol{q}$ is a normalization (column) vector. The modeling with the ODF approach is very effective for capturing the uncertainties because the material properties can be computed using the volume-averaged (homogenization) equations that are linear in the ODFs according to the Taylor approximation [32]. Therefore the uncertainty propagation to the material properties can also be computed with linear relations using the Gaussian feature.

The ODF is represented using a d-dimensional multivariate Gaussian distribution: $\boldsymbol{A} \sim \boldsymbol{N}(\boldsymbol{\mu}_A, \Sigma_A)$, where $\boldsymbol{\mu}_A$ is a vector of mean values of the ODF at independent nodes such that $\boldsymbol{\mu}_A = (\mu_1, \ldots, \mu_k)^T = E[\boldsymbol{A}]$ and Σ_A is the covariance matrix, $\Sigma_{A_{ij}} = \mathrm{cov}(A_i, A_j) = E[(A_i - \mu_{A_i})(A_j - \mu_{A_j})]$, $i, j = 1, \ldots, k$. In our previous work [7], it is shown that the volume-averaged material properties are linearly related to the ODF. For example, Eq. (3) can be generalized to a matrix–vector product, $\boldsymbol{Z} = \boldsymbol{P}\boldsymbol{A}$, that is also Gaussian: $\boldsymbol{Z} \sim \boldsymbol{N}(\boldsymbol{\mu}_Z, \Sigma_Z)$. The mean and covariance of vector $\boldsymbol{Z}$ are given by:

$$\boldsymbol{\mu}_Z = \boldsymbol{P}\boldsymbol{\mu}_A \tag{4}$$

$$\Sigma_Z = \boldsymbol{P}\Sigma_A \boldsymbol{P}^T \tag{5}$$

Using the same idea, the uncertainties in the material properties can be computed with the following relations given the ODF uncertainties.

$$\boldsymbol{q}^T \boldsymbol{\mu}_A = 1 \tag{6}$$

$$\boldsymbol{q}^T \Sigma_A \boldsymbol{q} = 0 \tag{7}$$

$$\boldsymbol{p}^T \boldsymbol{\mu}_A = \boldsymbol{\mu}_C \tag{8}$$

$$\boldsymbol{p}^T \Sigma_A \boldsymbol{p} = \Sigma_C \tag{9}$$

where Eqs. (6) and (7) show the ODF normalization constraint as applied for the Gaussian distribution. Equation (8) shows the formulation to obtain the vector of mean values of the properties, μ_C, using the linear transformation rule for Gaussian distribution [Eq. (4)] and the homogenization equation. Equation (9) shows the computation of the covariance matrix for the properties using linear transformation rule for Gaussians [Eq. (5)]. More details on Gaussian uncertainty representation of the ODFs can be found in our earlier works [5–7] and are not repeated here for brevity.

C. Example: Synthesis and UQ for a Colored Microstructure Movie

The uncertainties arising from the stochastic nature of the MRF approach are analyzed initially for an example problem that was studied previously in our study [20] for optimum window size determination. The example problem consists of a 2D microstructure generated from a cellular automata method [33]. The microstructure reconstruction was performed for window sizes of 5, 7, and 9 and the window size of 9 was found to provide the optimum result among all options by analyzing the results shown in Fig. 4.

The reconstructed microstructures were already compared with the original samples taken from the input colored movie at different times using statistical measures such as grain area and perimeter statistics and rose of interactions [20]. Therefore the microstructure reconstruction with different window sizes is not discussed in this study. Instead, the focus here is to model the epistemic uncertainties that introduced with the MRF algorithm. To generate statistical data 100 synthesized images are reconstructed at the final time step of the movie using the MRF method with the optimum fixed window size of 9. The size of the original image is 87×106 pixels, and the synthesized images are twice the size of the original. Generating synthesized microstructures over a larger domain compared with the

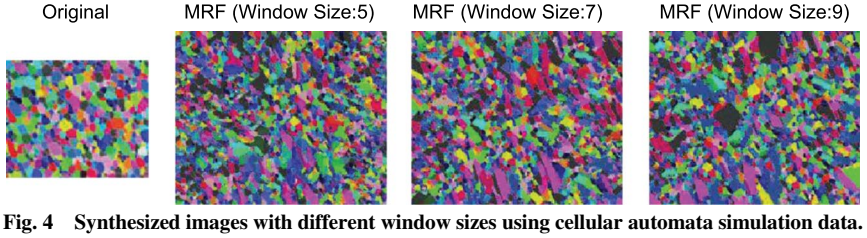

Fig. 4 Synthesized images with different window sizes using cellular automata simulation data.

input samples is important because if the computational model predicts the microstructural evolution accurately, then it would provide a huge cost reduction as the experiments over larger domains can be avoided.

Given a microstructure sample the ODF can be computed by assigning an orientation to each color in the sample because the ODF, in principle, is equivalent to a color histogram and contains the volume density of each crystal orientation (color) in the Rodrigues fundamental region. Using the synthesized image samples the uncertainties in the ODF values are first identified. The ODFs in these samples have similar distributions but with slightly different magnitudes, and their probability distributions are found to agree with the Gaussian distribution. Therefore the uncertainty propagation to the material properties is investigated by computing the probability distributions of these properties using the analytical UQ algorithm discussed in the previous section. In this example the material is an FCC copper polycrystal, and the values of the elastic parameters for a copper crystal are taken as [31]: $C_{11} = 168.0$ GPa, $C_{12} = 121.4$ GPa, and $C_{44} = 75.4$ GPa. The polycrystal stiffness $\boldsymbol{C}$ is computed through a weighted average of the stiffness of individual crystals expressed in the sample reference frame over the fundamental region. The material is modeled using 10 independent nodal points. However, the synthesized microstructure samples indicate eight number of strongly nonzero ODF parameters, whereas the other two ODF values are positive but they have negligible magnitudes. Therefore the probability distributions of these eight strongly nonzero ODF values are visualized in Fig. 5. The probability distributions of the stiffness parameters are shown in Fig. 6.

As illustrated by Figs. 5 and 6 the analytical UQ model captures the entire variability of the ODFs and stiffness parameters in the synthesized images. Even though the real MRF samples do not show a perfectly Gaussian distribution feature the analytical model is still able to represent all the uncertainty intervals, including the extreme (minimum and maximum) points. Therefore the analytical model is said to be reliable in this example with a simple visual check as it can predict the most extreme behaviors that are seen due to the epistemic uncertainties in the MRF approach. The uncertainties on the material properties can also be represented in terms of an "uncertainty closure," which is a convex hull showing all possible values of the material properties of interest. Generating the uncertainty hull is significant for material design because it shows how the values of engineering properties can differ from the deterministic values. An example computation is given in Fig. 7, which shows the convex hull of all possible C_{11}, C_{12}, and C_{22} values of MRF samples and analytical UQ solution. This figure shows that a designer should expect to see any value inside this convex hull for the stiffness parameters if the microstructural evolution is predicted with the MRF approach using the given input simulation data. The likelihood of any point occurrence in this domain is measured by the computed joint probability distributions. The analytical algorithm is said to be reliable by also looking at Fig. 7 because it has entirely covered the uncertainty domain of the MRF samples. The microstructure reconstruction will be performed using experimental data, and the uncertainty results will be compared with the measurements in the next section.

III. Quantification of Epistemic Uncertainties with Experimental Input Data

The analytical UQ algorithm has performed satisfactorily in the previous example discussed in Sec. II.C when the input data are taken from a cellular automata simulation. However, the uncertainty bounds have not been compared against measurements. Therefore this result leads us to another question: "Can the analytical UQ algorithm perform satisfactorily when the input is an experimental measurement?" The goal of this section is to analyze the uncertainties in the MRF samples to answer this question. The EBSD samples of a titanium–aluminum alloy (Ti-7Al) is used as the experimental input data. These samples were subject to the same thermomechanical process. All samples were compressed to 20% height reduction at room temperature, and annealed for 72 h at 1073 K. The compression direction is also the longitudinal direction of the forging. The microstructures were fully recrystallized at these conditions. Scans were taken from different regions of the processed samples. Each of the EBSD samples has an image size of 193×193 pixels, and the microstructure reconstruction is performed in two different domains: the first set of the synthesized images has the same image size with the EBSD samples, and the second set has 1.5 times larger image size than the EBSD data. Therefore the results of the first set are expected to provide an initial understanding such that if replacing experiments can be possible with the MRF approach. The results of the second set extend this understanding and show what happens when the MRF model generates larger-scale data than the experimental input.

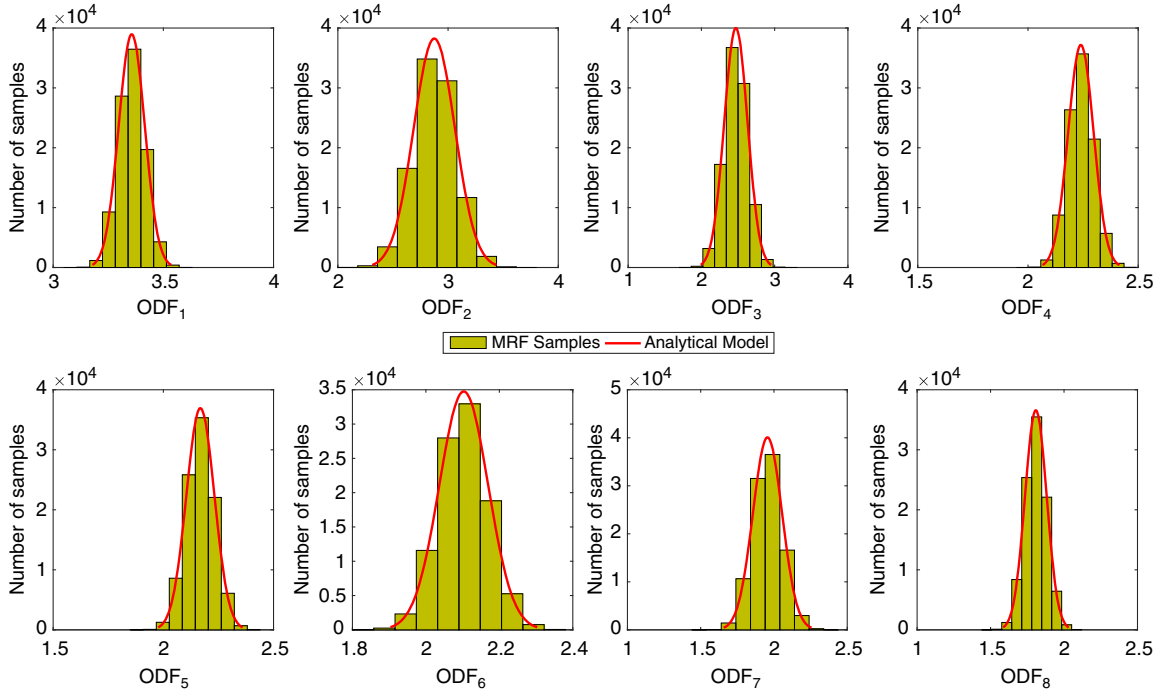

Fig. 5 Variations in the ODF parameters (green bars indicate ODF values that are calculated by using 100 MRF samples; red curves illustrate analytically calculated Gaussian probability distributions).

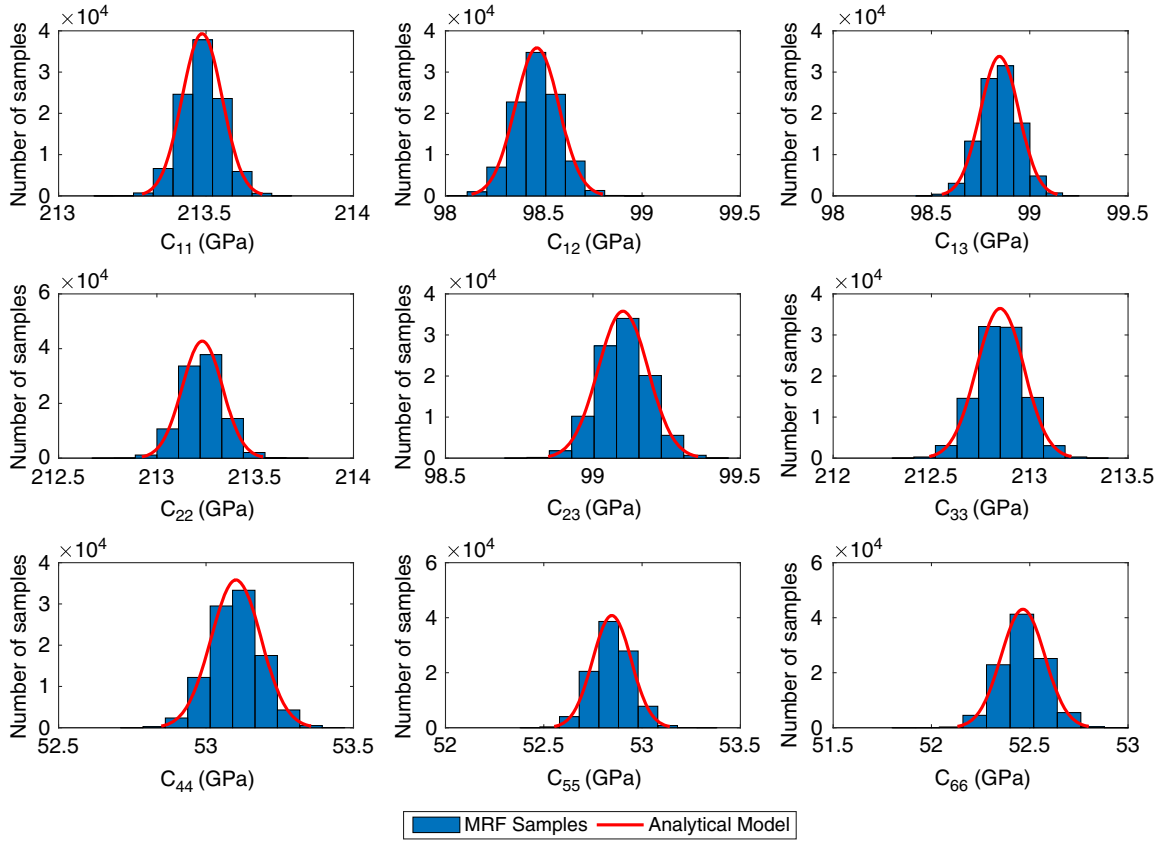

Fig. 6 Variations in stiffness parameters (blue bars indicate stiffness values that are calculated by using 100 MRF samples; red curves illustrate analytically calculated Gaussian probability distributions).

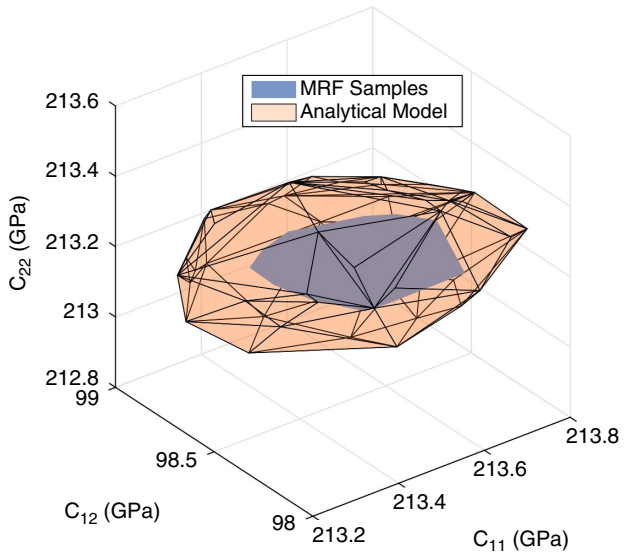

Fig. 7 Uncertainty closure for C_{11}, C_{12}, and C_{22}.

To analyze the uncertainties 100 MRF samples are generated from each EBSD image for each case. The original EBSD samples are visualized with example synthesized images for the same and larger image sizes in Fig. 8. Note that Fig. 8 illustrates two example synthesized images for each case (same or larger image size) per each of four input EBSD samples.

The material properties of interest in this application are not only the stiffness parameters but also the yield stress values at different strain offsets because the yield stress is more sensitive to the microstructural uncertainties. The property matrices for stiffness and yield stress values are obtained using the single crystal values presented in our previous work [34]. The probability distributions of the material properties computed using the MRF samples can also be compared with the experimental values. This is possible because the ODFs can directly be computed from the EBSD images as each different color in an EBSD sample corresponds to a different orientation. Therefore the volume fraction of each color in an EBSD sample relates to the ODF value of that particular orientation. Using the same volume averaging equations the material property values can be identified using the EBSD samples, and the performance of the MRF samples can be measured against these experimental values. For measuring the similarity between the probability distributions computed with the analytical UQ algorithm and the data represented by the MRF samples, a reliability index approach is used. There are some well-known similarity measurements available in literature such as Bhattacharyya distance [35] and Hellinger distance [36]. These measurements are beneficial when both sides of the data agree on either discrete or continuous probability distributions. However, in this application one data set indicates a continuous probability distribution (analytical UQ) and the other represents a discrete distribution (MRF samples). To measure the similarity between these two different data representations, the reliability index approach is found to be more convenient. Another advantage of this approach is that the reliability index can directly give information about how large an experimental data domain can reliably be captured by the MRF approach.

A. Results of Epistemic Uncertainty Analysis for the Same Image Size

The epistemic uncertainties arising from the MRF approach are first analyzed when the synthesized images have the same image size (193 × 193 pixels) with the experimental EBSD samples. The image reconstruction was repeated 100 times for each of the EBSD samples, resulting 400 samples generated by the MRF approach. To quantify the epistemic uncertainties the effect of aleatoric uncertainties are first eliminated from the EBSD data. This elimination is possible because all four input EBSD samples were measured from the same

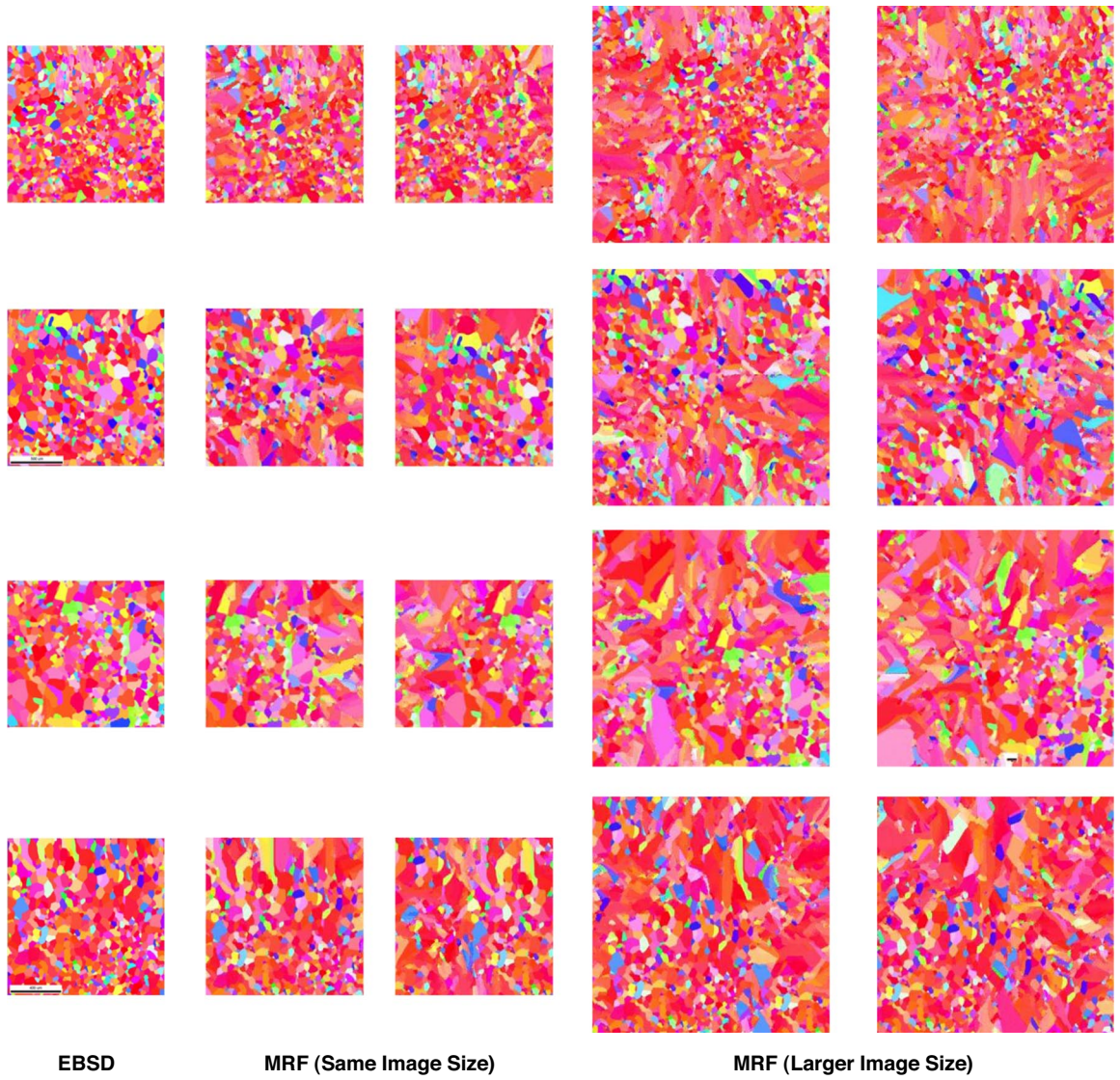

Fig. 8 Experimental EBSD samples and example MRF synthesized images.

material, but from different regions, which causes aleatoric uncertainties. Therefore the ODF and material property values of all four EBSD samples are calculated, and the MRF approach is considered to be 100% reliable if it produces results in between experimental values. The probability of failure for the MRF samples is computed by considering the regions that are outside of the experimental points. The epistemic uncertainties are analyzed for stiffness parameters and yield stress values at different strain offsets (0.2%, 1%, 2%, 5%, and 10% strains). The introduction of the yield stress parameter is important because it is more sensitive to the uncertainties than the stiffness properties. The probability distributions of the stiffness parameters that are computed using the 400 MRF samples are shown in Fig. 9. In Fig. 9, the blue bars are showing the material property values of the MRF samples, the red curve represents the probability distribution of the analytical UQ approach, and the black lines represent the experimental values that are computed using the four input EBSD images. It can be clearly seen that the analytical UQ algorithm provides a very good estimate to the MRF samples for the probability distributions of the stiffness parameters. A similar plot is also given in Fig. 10 to show the probability distributions of the yield stress values measured at different strain points by using the 400 MRF samples. The results in Fig. 10 also show that the analytical UQ algorithm is very good at capturing the variations in the MRF samples. Another important result that can be noticed in Figs. 9 and 10 is that the variations arising from the epistemic uncertainties of the MRF approach do not cause a significant deviation from the experimental values. From a visual check it can be observed that the limits of the EBSD samples shown by the black lines in Figs. 9 and 10 are mostly within the bounds defined by the MRF samples and corresponding analytical UQ results. The effect of epistemic uncertainties on the MRF approach as well as the accuracy of the analytical UQ technique to represent the MRF data are analyzed further by implementing a reliability index approach in Sec. III.C.

B. Results of Epistemic Uncertainty Analysis for the Larger Image Size

A second set of synthesized images were generated by inputting the same 4 EBSD samples. In this case a total of 400 MRF samples were reconstructed for 1.5 times larger image size (290×290 pixels) than the original EBSD data. This analysis holds another importance as it can reveal the accuracy of the MRF approach when it predicts over larger regions of experimental input data. The accuracy of predicting over larger domains is significant because it is less costly when the experiments are performed at smaller scales. Therefore the high accuracy of the MRF-based technique in predicting microstructural features as well as material properties by using smaller-scale experimental data would be advantageous in terms of eliminating the high costs of large-scale experiments.

The probability distributions that are computed using the 400 MRF samples for the stiffness parameters and yield stress values measured at different strain offsets (0.2%, 1%, 2%, 5%, and 10% strains) by using a larger image size are shown in Figs. 11 and 12. The analytical

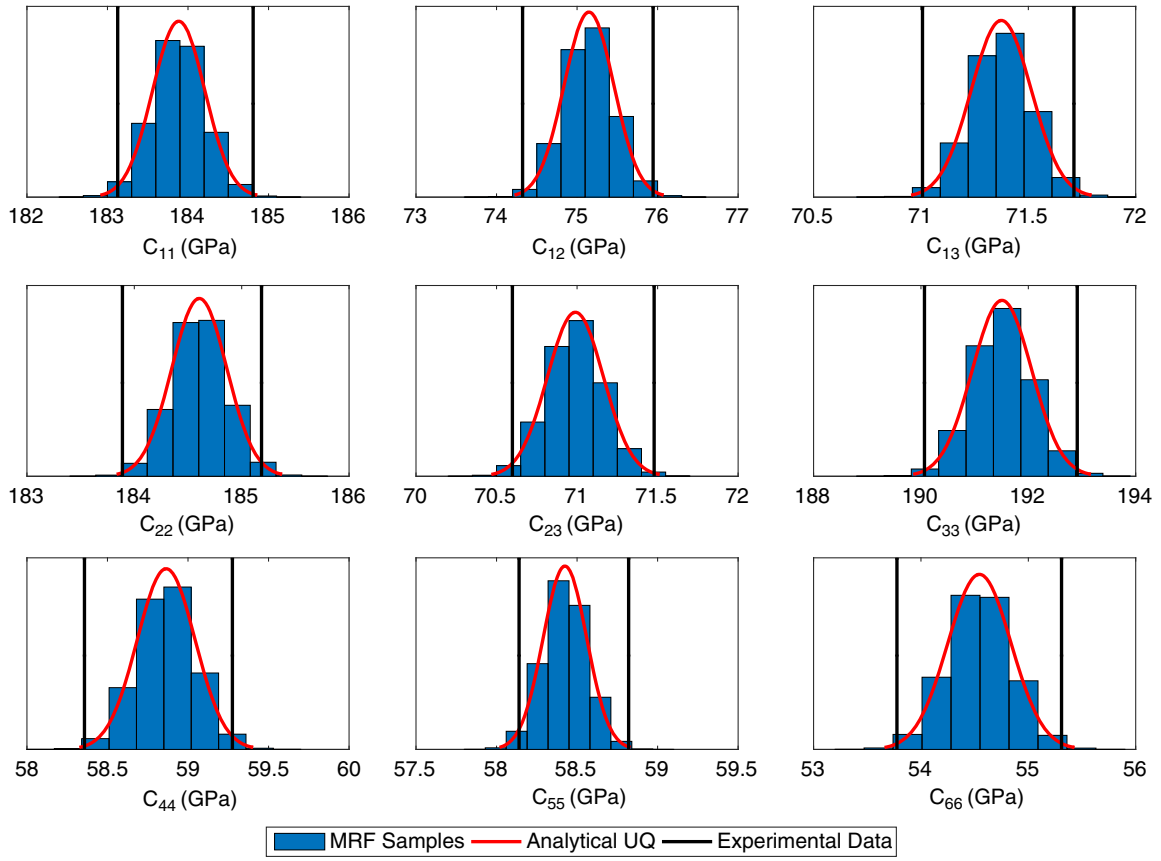

Fig. 9 Variations in stiffness parameters (blue bars indicate stiffness values that are calculated by using 400 MRF samples generated for the same EBSD image size, red curves illustrate analytically calculated Gaussian probability distributions using the MRF samples, and black lines show the experimental values computed using the EBSD images).

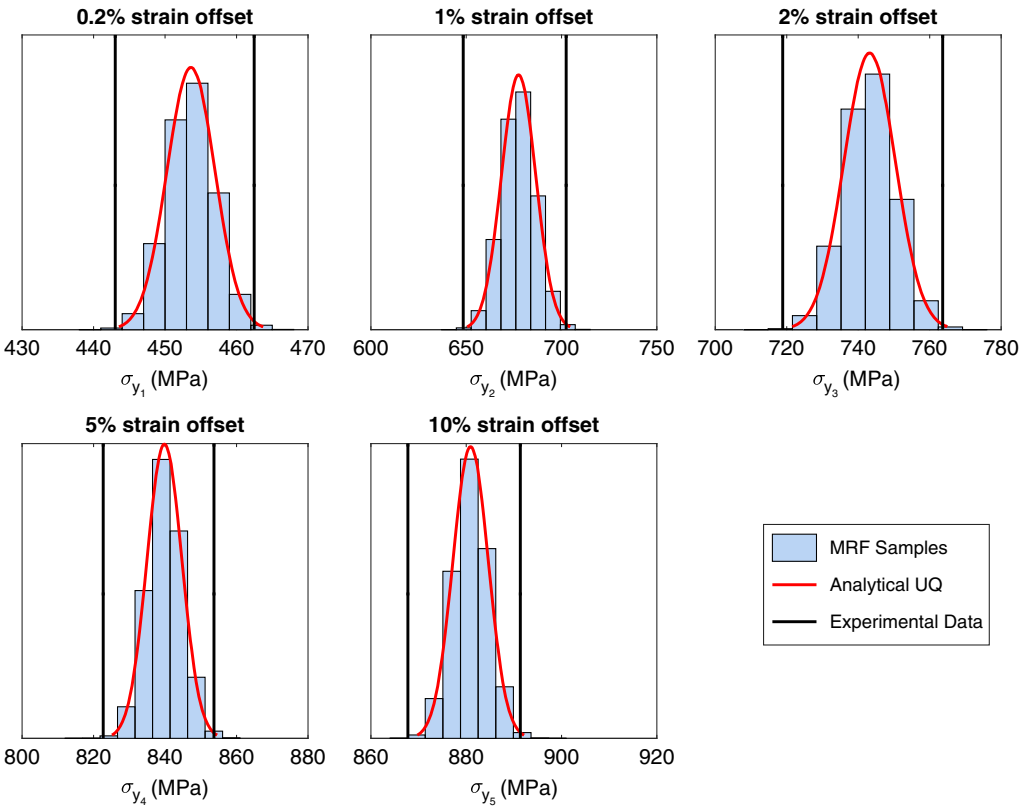

Fig. 10 Variations in yield stress values measured at different strain offsets (gray bars indicate yield stress values that are calculated by using 400 MRF samples generated for the same EBSD image size, red curves illustrate analytically calculated Gaussian probability distributions using the MRF samples, and black lines show the experimental values computed using the EBSD images).

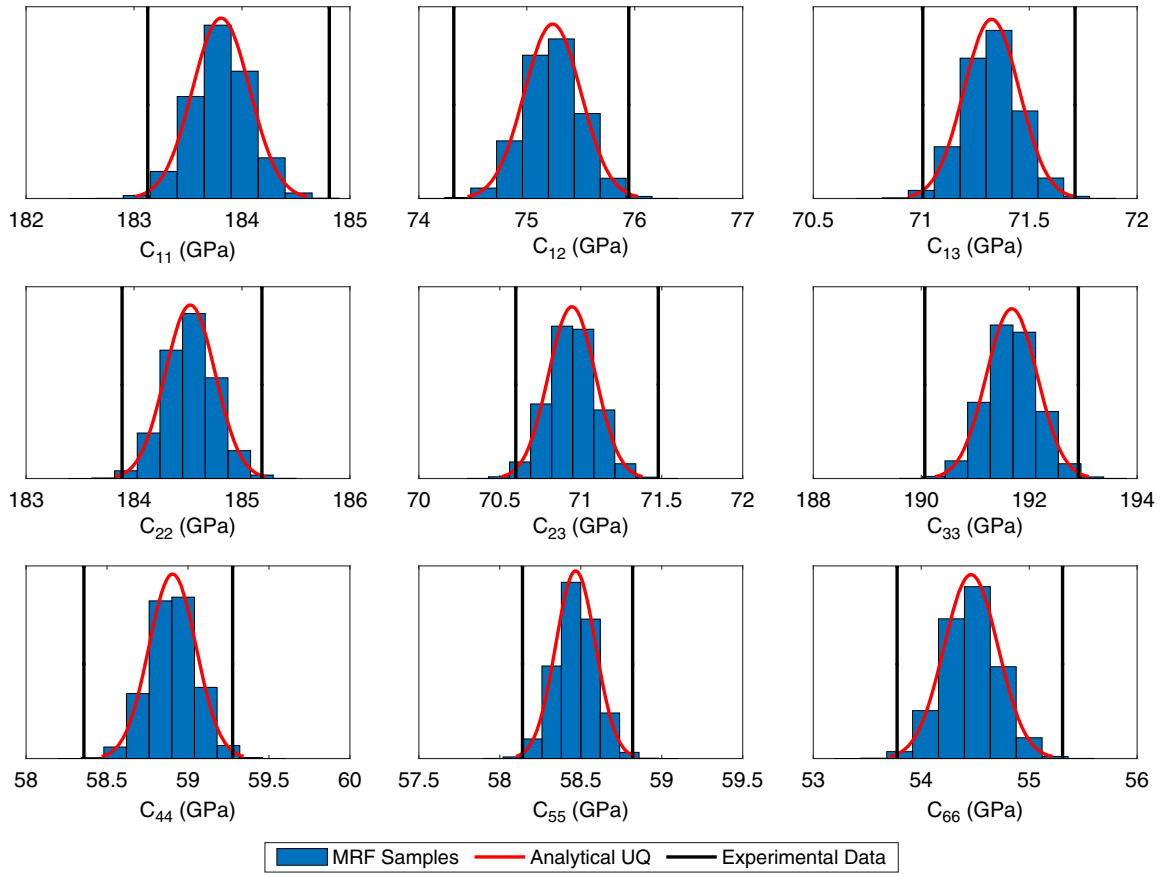

Fig. 11 Variations in stiffness parameters (blue bars indicate stiffness values that are calculated by using 400 MRF samples generated for 1.5 times larger EBSD image size, red curves illustrate analytically calculated Gaussian probability distributions using the MRF samples, and black lines show the experimental values computed using the EBSD images).

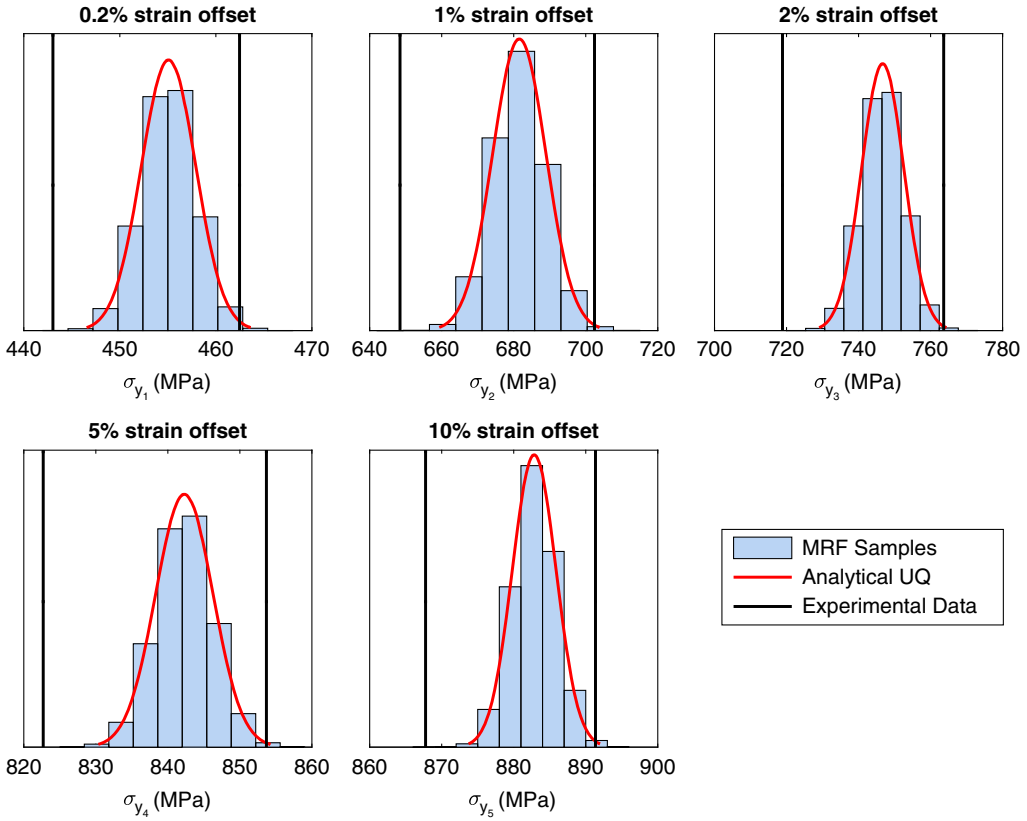

Fig. 12 Variations in yield stress values measured at different strain offsets (gray bars indicate yield stress values that are calculated by using 400 MRF samples generated for 1.5 larger EBSD image size, red curves illustrate analytically calculated Gaussian probability distributions using the MRF samples, and black lines show the experimental values computed using the EBSD images).

UQ algorithm is again very good at capturing the variations of the MRF samples as shown by Figs. 11 and 12. Even for the larger image size problem the MRF-based approach is again mostly within the limits of the experimental values, revealing that the epistemic uncertainties are not critical. The mathematical analysis of the epistemic uncertainties in this case as well as the accuracy of the analytical UQ technique to represent the variations of the synthesized samples are presented in Sec. III.C.

C. Reliability Index Approach

This section discusses a mathematical approach to analyze the effect of epistemic uncertainties arising from the MRF approach and the accuracy of the analytical UQ approach to predict the variations of the synthesized samples. This mathematical approach requires a technique to measure similarity between discrete data–discrete data and discrete data–continuous probability distribution because the effects of epistemic uncertainties are analyzed by comparing the MRF samples to the experimental values (discrete data–discrete data), and the accuracy of the analytical UQ algorithm is studied by measuring the similarity between the MRF samples and analytical probability distributions (discrete data–continuous probability distribution). The available numerical similarity measures focus more on comparing either discrete–discrete or continuous–continuous distributions. Therefore a reliability index approach that is capable of computing probability of failure for both discrete and continuous data sets is presented in this section instead of implementing an available numerical similarity test. The reliability index β is computed using the normal cumulative distribution function for the analytical UQ algorithm in Eq. (10).

$$\beta = \text{nor min } v(P(A \le x \le B)) \tag{10}$$

In Eq. (10), $P(A \le x \le B)$ shows the probability of having a random parameter, x, in between points A and B. The experimental value limits shown by the black lines in Figs. 9–12 denote the points A and B. The norminv function in Eq. (10) is the inverse Gaussian cumulative distribution function because the analytical UQ represents a Gaussian distribution. The definition for the norminv function is given in Eq. (11):

$$\text{norminv} = F^{-1}(P|\mu,\sigma) = \{x{:}F(x|\mu,\sigma) = P\} \tag{11}$$

where F^{-1} denotes the inverse function (norminv) of the normal cumulative function F; μ and σ are the mean value and standard deviation of the distribution, respectively; and P shows the probability.

The computation of the reliability index for a discrete data set is based on the computation of the probability of failure value, P_f. The probability of failure indicates the ratio of number of failed samples that are outside of the region defined by the points A and B over the total number of samples as shown in Eq. (12):

$$P_f = \frac{N_f}{N} \tag{12}$$

where N_f shows the number of failed samples and N is the total number of samples. The reliability index of the discrete system is then computed using the norminv function such that

$$\beta = \text{norminv}(1 - P_f) \tag{13}$$

To analyze the epistemic uncertainties the reliability index parameter β is found to be more preferable than the probability of failure parameter P_f because the probability of failure values is usually very small (in the order of 0.01). However, the reliability index parameter β can provide a better understanding as its values are very sensitive to the small changes in the probability of failure (the range for β is typically in between 1 and 3.5). Using the presented formulation, the reliability index values are computed for analytical UQ algorithm and MRF samples for the same and larger image sizes in Fig. 13. The reliability index that is calculated for the analytical UQ model indicates the accuracy of the technique to capture the variations of the MRF samples, whereas the reliability index of the MRF samples shows the importance of the epistemic uncertainties. Because the analytical UQ algorithm represents the MRF samples, these two reliability indexes are expected to be similar. To provide a better understanding of the reliability index values, the 90%, 95%, and 99% confidence (or reliability) levels are also illustrated in Fig. 13.

One important result that can be observed from Fig. 13 is that the analytical UQ algorithm never overpredicts the reliability because, in most cases, the reliability index value computed for the analytical technique is lower than the reliability index value for the discrete MRF samples. These two sets of reliability indexes have very similar values as expected, which shows the accuracy of the analytical UQ approach in modeling the variations of the MRF samples. Therefore the analytical algorithm is a very safe candidate to represent the epistemic uncertainties. The reliability index values in Fig. 13 are

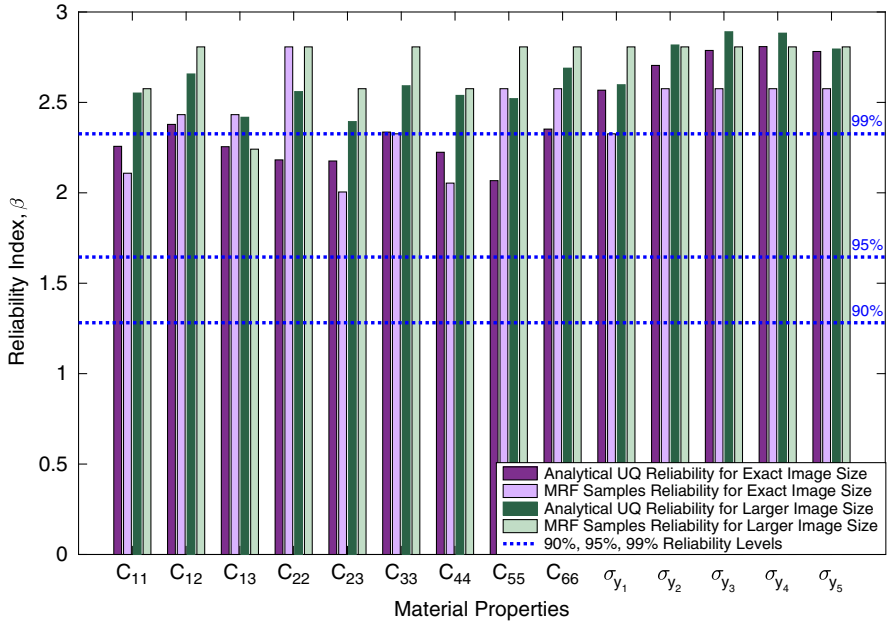

Fig. 13 Reliability of analytical UQ method and MRF samples based on the experimental EBSD data for the same and larger image sizes.

Table 1 Required computational times for different window size values in the MRF approach

Case	Computational time ratio per one sample
Same image size, window size of 5	1
1.5 times larger image size, window size of 5	2.24
Same image size, window size of 9	3.34
1.5 times larger image size, window size of 9	7.57

satisfactory because the confidence level is more than 95% in all cases and 99% in most of the cases. This also means that the epistemic uncertainties arising from the MRF approach have a very little impact on the overall accuracy of the algorithm even though the algorithm predicts the spatial evolution in a larger domain. The high confidence levels show that the MRF algorithm should be a very good candidate to replace the costly experimental data that are obtained with the measurements at large domains.

D. Effect of Window Size Parameter

The window size is the most effective parameter in terms of the accuracy of the synthesized images with the MRF approach. The UQ analysis in this work is performed using the synthesized images that are all generated for a window size of 9. This window size value was previously found to be optimum in the first application problem that was solved by using a cellular automata simulation output. Based on the results presented previously, this window size value also looks to be very effective on generating synthesized image samples from experimental EBSD data as the epistemic uncertainties arising from the MRF model do not violate the reliability expectations. This section focuses on a different analysis of epistemic uncertainties when different window size values are used in the MRF approach. For this purpose, another set of total 800 synthesized images (400 samples for the same image size and 400 samples for 1.5 times larger image size) are generated using the same input EBSD data but for a window size value of 5. Another important difference between using different window size values is the required computational times. The computational times that were spent to generate one synthesized image using the same and 1.5 larger image sizes with window sizes of 5 and 9 on the same computational platform are compared in Table 1. The computational time that was required by the analysis with a window size of 5 is significantly less than the required computational time with a window size of 9. However, the accuracy that is achieved by different window sizes may not be reflecting the same characteristic because there is a different optimal window size for each different problem depending on the crystal structure. Therefore spending more computational times may not mean achieving the best accuracy, which makes the MRF approach more attractive because it can produce accurate results in a computational time-efficient way. The only problem that can be noticed from the results in Table 1 is that the computational time that is required by the MRF approach to generate a 1.5 times larger image is more than 1.5 times of the computational time to generate an image having the same size with the input sample. Therefore the growth in computational time requirement is not linear, and it can cause some restriction for generating very big synthesized images. However, the probability of having an issue because of the computational time requirement is negligible considering the current high-technology computing resources.

Some of the material property values of the synthesized samples that are generated for the window size of 5 are compared with the previously generated images with the window size of 9 in Fig. 14. Figure 14 represents the property hulls of some of the stiffness parameters for the same and larger image sizes, and it shows all possible values that the synthesized MRF samples with different window size parameters can take.

The stiffness hulls in Fig. 14 show that the MRF samples that are generated using the window size of 5 predict very similar stiffness values to the previously synthesized images with the window size of 9. The similarity of the synthesized images with different window size values is analyzed further with the reliability index approach. The reliability index values are computed using the same formulation presented in the previous section. In this case, only the reliability indexes of the analytical UQ algorithm are illustrated because it is already shown that they agree very well with the reliability indexes of the discrete MRF samples. The reliability index values computed for the window size of 5 are compared with the previous reliability index values that were obtained for the window size parameter of 9 in Fig. 15.

According to the reliability results illustrated by Fig. 15 the reliability of the synthesized samples using a window size of 5 is as good as the samples generated with the window size of 9. The most reliability levels are above 99% confidence, and all samples are providing a reliability more than 95%. Even though the window size parameter is important for the accuracy of the MRF samples it is not critical in this example application. The reason is that the experimental input EBSD images represent a microstructural texture that is very close to a perfect random texture. All the grains in this texture have regular shapes and similar sizes. Therefore the reconstruction can be very accurate even with small window sizes. The accuracy of the synthesized images with different window sizes for anisotropic grain structures has been discussed before by the authors [20]. The results of this previous study [20] showed that the window size parameter is significant when the grains have different structures in contrast to the results presented in this work for a random texture. However, the present study shows that the MRF approach is a very good candidate to eliminate the large-scale experiments that are performed for materials with regular grain structures. The replacement of the experiments with

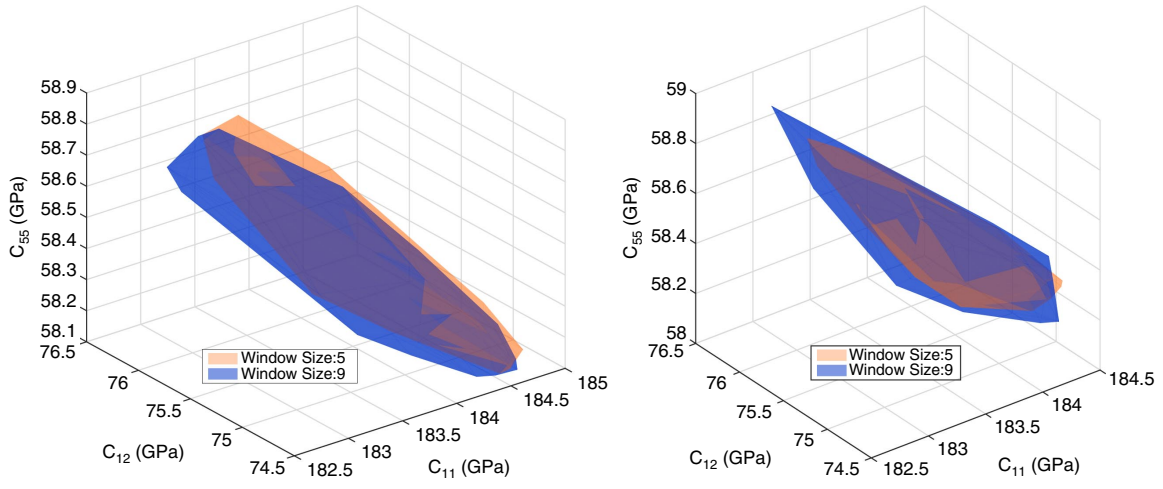

a) Same image size **b) Larger image size**

Fig. 14 Stiffness hulls for the synthesized MRF samples with different window sizes.

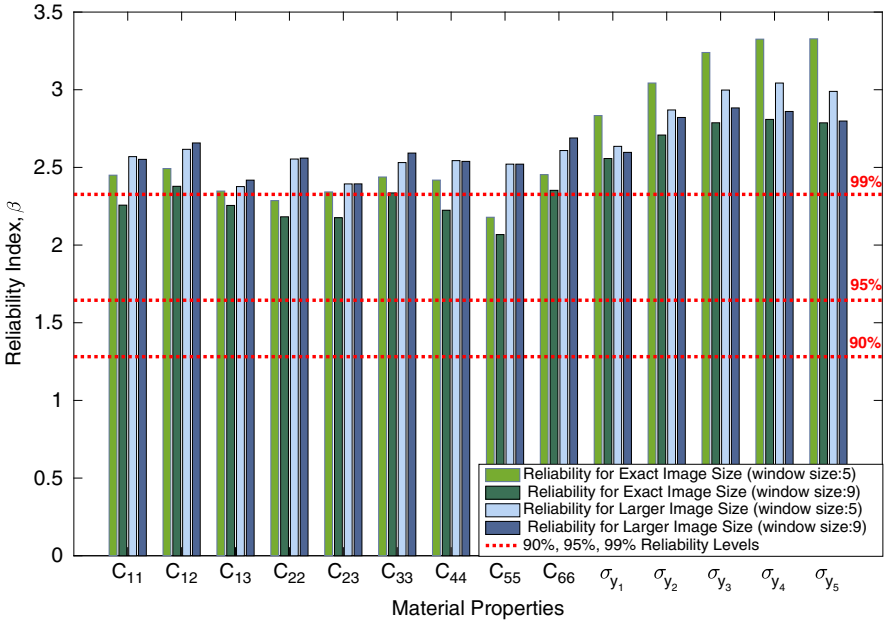

Fig. 15 Reliability of analytical UQ method for the same and larger image sizes using different window sizes.

the MRF approach for anisotropic microstructures should be studied more extensively in future.

IV. Conclusions

An analytical formulation to model epistemic uncertainties that are arising from a microstructure reconstruction algorithm is addressed. The spatial evolution of synthetic microstructures is predicted by an Markov random field (MRF) model given an experimental electron backscatter diffraction (EBSD) input data. To understand the effects of epistemic uncertainties, the aleatoric uncertainties are eliminated by using four different EBSD samples that indicate measurements at different regions of the same material. The variations of the material properties that are computed from the EBSD samples are related to aleatoric uncertainties. Therefore the outputs that are produced by the MRF algorithm within the experimental property bounds are assumed to be reliable. The epistemic uncertainties are analyzed for the material property values that are not a subspace of the experimental values region. A reliability index approach is presented to compute the similarity between the analytical uncertainty quantification (UQ) algorithm and discrete MRF samples to show the accuracy of the analytical algorithm in modeling epistemic uncertainties, and between the analytical algorithm and discrete experimental values to show the effect of epistemic uncertainties on the expected performance of the MRF model. The analytical UQ algorithm is found to be providing a very good estimate for the variations in the MRF samples. Moreover, the reliability analysis shows that the epistemic uncertainties arising from the MRF algorithm do not lead to unexpected results because the confidence levels in all cases for different image and window sizes are more than 95%. The window size parameter does not play a significant role on the accuracy of the synthesized samples because the input experimental data represent a random texture. The future work should focus more on the development of techniques to identify the optimum window size parameter, which provides improvement on both accuracy and computational time, to analyze uncertainties when modeling microstructures with different grain structures over larger spatial domains.

Acknowledgments

The work presented here was funded by Office of Naval Research (ONR) grant N00014-12-1-0013. The authors would like to thank Anna Trump and John Allison (Materials Science and Engineering Department of University of Michigan) for providing the experimental data. The computations have been carried out as part of research supported by the U.S. Department of Energy, Office of Basic Energy Sciences, Division of Materials Sciences and Engineering, under Award No. DE-SC0008637, which funds the PRedictive Integrated Structural Materials Science (PRISMS) Center at the University of Michigan.

References

[1] Peters, M., Kumpfert, J., Ward, C. H., and Leyens, C., "Titanium Alloys for Aerospace Applications," *Advanced Engineering Materials*, Vol. 5, No. 6, 2003, pp. 419–427. doi:10.1002/adem.200310095

[2] Kindermann, R., and Snell, J. L., "Markov Random Fields and Their Applications, American Mathematical Society," Vol. 1, 1980. doi:10.1090/conm/001

[3] Creuziger, A., Syed, K., and Gnaupel-Herold, T., "Measurement of Uncertainty in Orientation Distribution Function Calculations," *Scripta Materialia*, Vols. 72–73, No. 1, 2014, pp. 55–58. doi:10.1016/j.scriptamat.2013.10.017

[4] Kouchmeshky, B., and Zabaras, N., "The Effect of Multiple Sources of Uncertainty on the Convex Hull of Material Properties of Polycrystals," *Computational Materials Science*, Vol. 47, No. 2, 2009, pp. 342–352. doi:10.1016/j.commatsci.2009.08.010

[5] Acar, P., Srivastava, S., and Sundararaghavan, V., "Stochastic Design Optimization of Microstructures with Utilization of a Linear Solver," *AIAA Journal*, Vol. 55, No. 9, 2017, pp. 3161–3168. doi:10.2514/1.J056000

[6] Acar, P., and Sundararaghavan, V., "Uncertainty Quantification of Microstructural Properties due to Experimental Variations," *AIAA Journal*, Vol. 55, No. 8, 2017, pp. 2824–2832. doi:10.2514/1.J055689

[7] Acar, P., and Sundararaghavan, V., "Uncertainty Quantification of Microstructural Properties due to Variability in Measured Pole Figures," *Acta Materialia*, Vol. 124, Feb. 2017, pp. 100–108. doi:10.1016/j.actamat.2016.10.070

[8] Heeger, D. J., and Bergen, J. R., "Pyramid-Based Texture Analysis/Synthesis," *SIGGRAPH 95*, Sept. 1995, pp. 229–238. doi:10.1145/218380

[9] Bonet, J. S. D., "Multiresolution Sampling Procedure for Analysis and Synthesis of Texture Images," *SIGGRAPH 97*, Aug. 1997, pp. 361–368. doi:10.1145/258734.258882

[10] Simoncelli, E. P., and Portilla, J., "Texture Characterization via Joint Statistics of Wavelet Coefficient Magnitudes," *Proceedings of 5th International Conference on Image Processing*, IEEE Publ., Piscataway, NJ, 1998. doi:10.1109/ICIP.1998.723417

[11] Torquato, S., "Random Heterogeneous Materials: Microstructure and Macroscopic Properties," Springer–Verlag, New York, 2002, pp. 23–58.

[12] Ising, E., "Beitrag zur Theorie des Ferromagnetismus," *Zeitschrift Physik*, Vol. 31, No. 1, 1925, pp. 253–258. doi:10.1007/BF02980577

[13] Shannon, C. E., "A Mathematical Theory of Communication," *Bell System Technical Journal*, Vol. 27, No. 3, 1948, pp. 379–423. doi:10.1002/bltj.1948.27.issue-3

[14] Efros, A., and Leung, T., "Texture Synthesis by Non-Parametric Sampling," *International Conference on Computer Vision*, Vol. 2, IEEE Publ., Piscataway, NJ, 1999, pp. 1033–1038. doi:10.1109/ICCV.1999.790383

[15] Popat, K., and Picard, R., "Novel Cluster-Based Probability Model for Texture Synthesis, Classification, and Compression," *Visual Communications and Image Processing*, Oct. 1993, pp. 756–768. doi:10.1117/12.157992

[16] Zhu, S., Wu, Y., and Mumford, D., "Filters, Random Fields and Maximun Entropy (FRAME)—Towards a Unified Theory for Texture Modeling," *International Journal of Computer Vision*, Vol. 27, No. 2, 1998, pp. 107–126. doi:10.1023/A:1007925832420

[17] Paget, R., and Longstaff, I., "Texture Synthesis via a Noncausal Nonparametric Multiscale Markov Random Field," *IEEE Transactions on Image Processing*, Vol. 7, No. 6, 1998, pp. 925–931. doi:10.1109/83.679446

[18] Mariethoz, G., and Lefebvre, S., "Bridges Between Multiple-Point Geostatistics and Texture Synthesis," *Computers & Geosciences*, Vol. 66, No. C, 2014, pp. 66–80. doi:10.1016/j.cageo.2014.01.001

[19] Kumar, A., Sundararaghavan, V., DeGraef, M., and Nguyen, L., "A Markov Random Field Approach for Microstructure Synthesis," *Modelling and Simulation in Materials Science and Engineering*, Vol. 24, No. 3, 2016, pp. 035015–13. doi:10.1088/0965-0393/24/3/035015

[20] Acar, P., and Sundararaghavan, V., "A Markov Random Field Approach for Modeling Spatio-Temporal Evolution of Microstructures," *Modelling Simulation Materials Science and Engineering*, Vol. 24, No. 7, 2016, Paper 075005. doi:10.1088/0965-0393/24/7/075005

[21] Kwatra, V., Essa, I., Bobick, A., and Kwatra, N., "Texture Optimization for Example-Based Synthesis," *ACM Transactions on Graphics (Proc. SIGGRAPH)*, Vol. 24, No. 3, 2005, pp. 795–802. doi:10.1145/1073204

[22] Kopf, J., Fu, C.-W., Cohen-Or, D., Deussen, O., Lischinski, D., and Wong, T.-T., "Solid Texture Synthesis from 2D Exemplars," *SIGGRAPH Proceedings*, Vol. 2, Aug. 2007, pp. 1–9. doi:10.1145/1276377.1276380

[23] Sundararaghavan, V., "Reconstruction of Three Dimensional Anisotropic Microstructures from Two-Dimensional Micrographs Imaged on Orthogonal Planes," *Integrating Materials and Manufacturing Innovation*, Vol. 3, No. 19, 2014, pp. 1–11. doi:10.1186/s40192-014-0019-3

[24] Sundararaghavan, V., and Zabaras, N., "Classification and Reconstruction of Three-Dimensional Microstructures Using Support Vector Machines," *Computational Materials Science*, Vol. 32, No. 2, 2005, pp. 223–239. doi:10.1016/j.commatsci.2004.07.004

[25] Yeong, C. L. Y., and Torquato, S., "Reconstructing Random Media II. Three-Dimensional Media from Two-Dimensional Cuts," *Physical Review E*, Vol. 58, No. 1, 1998, pp. 224–233. doi:10.1103/PhysRevE.58.224

[26] Manwart, C., Torquato, S., and Hilfer, R., "Stochastic Reconstruction of Sandstones," *Physical Review E*, Vol. 62, No. 1, 2000, pp. 893–899. doi:10.1103/PhysRevE.62.893

[27] Besag, J., "Spatial Interaction and the Statistical Analysis of Lattice Systems," *Journal of the Royal Statistical Society Series B (Methodological)*, Vol. 36, No. 2, 1974, pp. 192–236.

[28] Wei, L.-Y., Lefebvre, S., Kwatra, V., and Turk, G., "State of the Art in Example-Based Texture Synthesis," State of the Art Report, EG-STAR, Eurographics, 2009. doi:10.2312/egst.20091063

[29] Kumar, A., and Dawson, P. R., "Computational Modeling of F.C.C. Deformation Textures over Rodrigues' Space," *Acta Materialia*, Vol. 48, No. 10, 2000, pp. 2719–2736. doi:10.1016/S1359-6454(00)00044-6

[30] Sundararaghavan, V., and Zabaras, N., "A Multi-Length Scale Sensitivity Analysis for the Control of Texture-Dependent Properties in Deformation Processing," *International Journal of Plasticity*, Vol. 24, No. 9, 2008, pp. 1581–1605. doi:10.1016/j.ijplas.2007.12.005

[31] Sundararaghavan, V., and Zabaras, N., "Linear Analysis of Texture-Property Relationships Using Process-Based Representations of Rodrigues Space," *Acta Materialia*, Vol. 55, No. 5, 2007, pp. 1573–1587. doi:10.1016/j.actamat.2006.10.019

[32] Taylor, G. I., "Plastic Strain in Metals," *Journal of the Institute of Metals*, Vol. 62, May 1938, pp. 307–324.

[33] Max Planck Institut fur Eisenforschung, "Cellular Automaton Simulations of Grain Growth, Recrystallization," www.youtube.com/watch?v=NhfRaLUtvBQ [retrieved 17 Feb. 2016].

[34] Acar, P., Ramazani, A., and Sundararaghavan, V., "Crystal Plasticity Modeling and Experimental Validation with an Orientation Distribution Function for Ti-7Al Alloy," *Metals*, Vol. 7, No. 11, 2017, pp. 459. doi:10.3390/met7110459

[35] Bhattacharyya, A., "On a Measure of Divergence Between Two Statistical Populations Defined by Their Probability Distributions," *Bulletin of the Calcutta Mathematical Society*, Vol. 35, 1943, pp. 99–109.

[36] Hellinger, E., "Neue Begrundung der Theorie quadratischer Formen von unendlichvielen Veranderlichen," *Journal fur die reine und angewandte Mathematik*, Vol. 136, 1909, pp. 210–271 (in German).

R. Ohayon
Associate Editor